Resonance Cones below the Ion Cyclotron Frequency: Theory and Experiment*

P. Bellan
Princeton University, Plasma Physics Laboratory, Princeton, New Jersey 08540
(Received 15 March 1976)

The resonance cones existing below the ion cyclotron frequency, ω_{ci}, are shown, theoretically and experimentally, to be the asymptotes of hyperbolic constant-phase surfaces of low-frequency ion acoustic waves. Above ω_{ci} the surfaces transform into ellipses that are related to the electrostatic ion cyclotron waves and ion acoustic waves.

Although the electrostatic *Fourier* modes, $\varphi(x,t)\sim\exp(i\vec{k}\cdot\vec{x}-i\omega t)$, in the ion cyclotron regime have been known for some time, there has not been, except for the work by Kuehl[1] and Burrell,[2] any attempt to make a detailed analysis of the wave field excited by a *point* source. This type of source may be thought of, mathematically, as the Green's function for the finite-size grids and probes commonly used to excite waves in laboratory plasmas.[3,4]

In general, point sources (and other finite sources) excite a broad spectrum of spatial Fourier modes $\sim e^{i\vec{k}\cdot\vec{x}}$. The total field of this broad spectrum does not necessarily correspond to the field of a monochromatic (single-$\vec{k}$) Fourier mode. Fisher and Gould,[5] while analyzing the resonant cone field of point sources in the electron plasma wave regime, pointed out that resonance cones should also exist at frequencies ω below the ion cyclotron frequency ω_{ci}. Kuehl[1] calculated the fields for $\omega<\omega_{ci}$ and finite T_e, and found the existence of resonant cones making an angle $\theta_c\sim\sin^{-1}(\omega/\omega_{ci})$ with respect to the confining magnetic field $\vec{B}$. Burrell[2] found a result similar to Ref. 1 and, for the case of $\omega_{ci}\gg\omega,\omega_{pi}$, considered the additional effect of finite T_i.

In this Letter we present the first experimental evidence of $\omega<\omega_{ci}$ resonance cone behavior. We further show, both theoretically and experimentally, that (1) the $\omega<\omega_{ci}$ resonance cones are the asymptotes of hyperbolic constant-phase surfaces and (2) for $\omega>\omega_{ci}$ these surfaces transform into ellipses which are related to both the electrostatic ion cyclotron waves and ion acoustic waves. For clarity and completeness we outline the derivation of the Green's function[1,2]; the properties of this function determine both the resonance cone behavior and the hyperbolic-to-elliptic transition described above.

Let us first briefly review the modes existing around $\omega=\omega_{ci}$. With the assumption $k_\parallel v_{T_i}\ll\omega\ll k_\parallel v_{T_e}$ the electrostatic dispersion relation becomes[6]

$$\epsilon(\vec{k},\omega)=1+\frac{1}{k^2\lambda_{De}^2}-\frac{\omega_{pi}^2}{\omega^2-\omega_{ci}^2}\frac{k_\perp^2}{k^2}-\frac{\omega_{pi}^2}{\omega^2}\frac{k_\parallel^2}{k^2}=0. \tag{1}$$

Equation (1) has two roots:

$$\omega_\pm^2=\left\{(\omega_s^2+\omega_{ci}^2)\pm\left[(\omega_{ci}^2+\omega_s^2)^2-4\omega_{ci}^2\omega_s^2\cos^2\xi\right]^{1/2}\right\}/2 \tag{2}$$

where $\omega_s^2=k^2c_s^2/(1+k^2\lambda_{De}^2)$, $\xi=\cos^{-1}(\vec{k}\cdot\vec{B}/kB)$ and the other symbols have their usual meanings. ω_+ lies above ω_{ci}, and ω_- lies below. For $\omega_s^2/\omega_{ci}^2\gg1$, $\omega_+^2\cong\omega_{ci}^2\sin^2\xi+\omega_s^2$ (ion acoustic wave) while $\omega_-^2\cong\omega_{ci}^2\cos^2\xi$ (second ion cyclotron wave). For $\omega_s^2/\omega_{ci}^2\ll1$, $\omega_+^2\cong\omega_{ci}^2+\omega_s^2\sin^2\xi$ (electrostatic ion cyclotron wave) while $\omega_-^2\cong\omega_s^2\cos^2\xi$ (low-frequency ion acoustic wave).

Let us now calculate the field excited by a test charge, q_t, oscillating at a frequency ω [where $\omega\sim O(\omega_{ci})\ll\omega_{pi}$]. The potential φ is given by

$$\varphi(x,t)=(2\pi)^{-3}\int d^3k\,\frac{4\pi q_t e^{i\vec{k}\cdot\vec{x}-i\omega t}}{k^2\epsilon(\vec{k},\omega)}. \tag{3}$$

Using the cylindrical coordinates $k_\parallel$, $k_\perp$, ψ and noting $\vec{k}\cdot\vec{x}=k_\parallel z+k_\perp\rho\cos\psi$, we find on performing the ψ integration

$$\varphi(x,t)=-\frac{q_t}{\pi\lambda_{De}d_\parallel}\int_0^\infty d\kappa_\perp\kappa_\perp J_0\left(\frac{\kappa_\perp\rho}{\lambda_{De}}\right)\int_{-\infty}^{\infty}d\kappa_\parallel\,\frac{\exp(i\kappa_\parallel z/\lambda_{De}-i\omega t)}{\kappa_\parallel^2-(\kappa_\perp^2d_\perp d_\parallel^{-1}+d_\parallel^{-1})}, \tag{4}$$

where $\kappa_\perp=k_\perp\lambda_{De}$, $\kappa_\parallel=k_\parallel\lambda_{De}$, $d_\parallel=\omega_{pi}^2/\omega^2-1$, and $d_\perp=1-\omega_{pi}^2/(\omega^2-\omega_{ci}^2)$. With use of the method of residues for the $\kappa_\parallel$ integration, the $\kappa_\perp$ integral becomes a Hankel transform, tabulated in Erdelyi *et al.*[7] Note that $d_\parallel>0$ always, but $d_\perp>0$ for $\omega^2<\omega_{ci}^2$ and $d_\perp<0$ for $\omega^2>\omega_{ci}^2$. For $\omega<\omega_{ci}$ Ref. 7 gives the

following simple results: (a) For $0<\rho^2/d_\perp<z^2/d_\parallel$,

$$\varphi(x,t)=\frac{q_t}{d_\parallel^{1/2}d_\perp}\frac{\exp[i(z^2/d_\parallel-\rho^2/d_\perp)^{1/2}/\lambda_{De}-i\omega t]}{(z^2/d_\parallel-\rho^2/d_\perp)^{1/2}}, \tag{5a}$$

(b) for $0<z^2/d_\parallel<\rho^2/d_\perp$,

$$\varphi(x,t)=\frac{-iq_t}{d_\parallel^{1/2}d_\perp}\frac{\exp[-(\rho^2/d_\perp-z^2/d_\parallel)^{1/2}/\lambda_{De}-i\omega t]}{(\rho^2/d_\perp-z^2/d_\parallel)^{1/2}}, \tag{5b}$$

where z and ρ are cylindrical coordinates. For $\omega>\omega_{ci}$, Ref. 7 shows that the potential is again given by Eq. 5(a), which is now valid for all ρ,z. [Equation 5(a) is similar to Eq. (20) of Ref. 1 and Eq. (21) of Ref. 2; however, $K_\perp^{(c)}$ of Ref. 1 should be replaced by $d_\perp$ since $\omega/k_\parallel v_{Te}\ll 1$, and there is also a minor difference of $(1-\omega^2/\omega_{pi})^{-1}$ in the phase.]

Equations 5(a) and 5(b) may be interpreted by examining the quantity $(z^2/d_\parallel-\rho^2/d_\perp)^{1/2}/\lambda_{De}$ in the limit $\omega_{pi}^2/\omega_{ci}^2\to\infty$. In this case

$$(z^2/d_\parallel-\rho^2/d_\perp)^{1/2}/\lambda_{De}\approx[1-(\omega_{ci}^2/\omega^2)\sin^2\theta]^{1/2}\omega r/c_s, \tag{6}$$

where $r=(z^2+\rho^2)^{1/2}$ and $\theta=\tan^{-1}(\rho/z)$. Note that θ, an angle in real space, is not the same as ξ, an angle in k space.

Equation (6) determines both the phase and the amplitude of Eq. (5), and thus shows how Eq. (5) is related to both the resonance cones and the dispersion relations discussed after Eq. (1). For $\omega<\omega_{ci}$, $d_\perp>0$ so that the surfaces of constant phase are hyperbolas, as shown in Fig. 1(a). There are resonant cones at the asymptotic angle of the hyperbolas $\theta_c\cong\sin^{-1}(\omega/\omega_{ci})$, since at this angle the quantity in Eq. (6) vanishes, causing the potential in Eq. (5a) to diverge.[1] For angles $\theta>\theta_c$, the waves, now described by Eq. (5b), are evanescent [evanescent region is shown in Fig. 1(a)]. For $\theta=0$ the waves obey the dispersion relation $\omega=kc_s$, with no resonance at $\omega=\omega_{ci}$. From the $\theta=0$ result it can be seen that the reason grids have worked well for parallel wave propagation experiments[3] is that they effectively enlarge the region where $\theta\approx 0$ [cf. Fig. 1(a)].

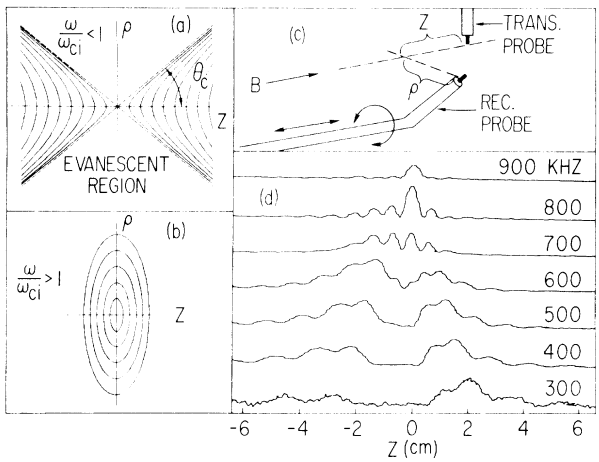

FIG. 1. (a) Constant-phase surfaces for $\omega/\omega_{ci}<1$. These are hyperbolas having asymptotes (dotted lines) at angle $\theta_c=\tan^{-1}(d_\perp/d_\parallel)^{1/2}\approx\sin^{-1}(\omega/\omega_{ci})$. For $\theta>\theta_c$ the wave is evanescent. (b) Constant-phase surfaces for $\omega/\omega_{ci}>1$. These are now ellipses. (c) Experimental setup. (d) Amplitude profiles; $f_{ci}=705$ kHz; $\rho=0.64$ cm.

In contrast, when $\omega>\omega_{ci}$, $d_\perp<0$, and Eq. (5a) now shows that the surfaces of constant phase are ellipses; cf. Fig. 1(b).

Our experiment was designed to show the existence of $\omega<\omega_{ci}$ resonance cone behavior and also to demonstrate the transition from $\omega/\omega_{ci}<1$ to $\omega/\omega_{ci}>1$. A probe, located at the center of the $L3$ plasma (He gas, $B=0.5$–2 kG, $n\sim10^{10}$ cm^{-3}, $T_e\sim2$–5 eV, $T_i<0.1$ eV, other parameters given in Bellan and Porkolab[8] and driven by an oscillator, excited waves either above or below ω_{ci}. The experimental setup is sketched in Fig. 1(c): Waves were picked up by an axially translatable probe that could also be rotated to have different radial displacements, ρ, from the transmitting probe (2–5 mm probe lengths were used; no dependence of field pattern on probe length over this range was noted).

Figure 1(d) shows, for $\rho=0.64$ cm and a sequence of frequencies, plots of wave amplitude versus z. (The modulation of the amplitude profiles comes from a beating of the wave with a simultaneously excited,[4] long-wavelength electromagnetic mode.) Below $\omega_{ci}/2\pi=705$ kHz the profiles have two peaks; these are the cones. As $\omega\to\omega_{ci}$ the cones move together, since θ_c [cf. Fig. 1(a)] is increasing. The cones have finite amplitude because the potential on the transmitting probe was finite; in the theory the potential on the point charge was infinite, so that the equipotential surfaces passing through the point charge

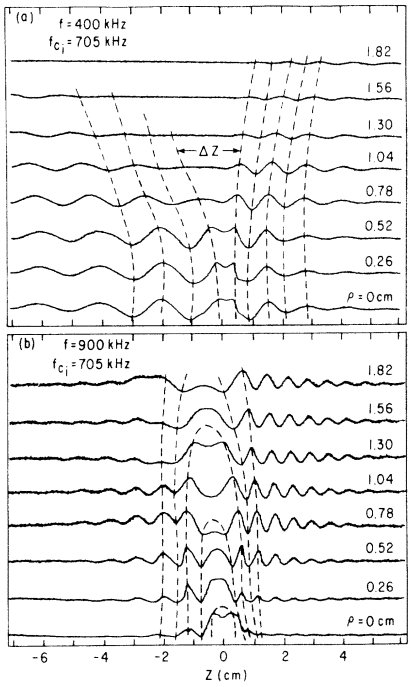

FIG. 2. (a). Interferometer signals for $\omega/\omega_{ci} = 0.57$. Constant-phase surfaces, shown by dashed lines, are hyperbolas. $B = 1.85$ kG; He gas. (b) Same as (a) except ω changed so that $\omega/\omega_{ci} = 1.28$. Constant-phase surfaces are now ellipses.

(i.e., the cones) were also infinite. [Inclusion of damping in the theory shows that the resonance varies as $(\omega/\nu_i)^{1/2}$; this also acts to keep the resonance finite.]

Measurements of the hyperbolic (elliptic) phase surfaces and θ_c were made using a standard interferometer system. Typical experimental results for fixed ω_{ci} and two values of ω are shown in Fig. 2. The constant-phase surfaces, shown by dashed lines in Figs. 2(a) and 2(b), clearly demonstrate the transition from hyperbolic behavior for $\omega < \omega_{ci}$ to elliptic behavior for $\omega > \omega_{ci}$, in agreement with the theory shown schematically in Figs. 1(a) and 1(b). Plasma drifting from the source (located on the right-hand side of Fig. 2) caused the axial asymmetry in Fig. 2. The effect of this drift was eliminated from measurements of the cone angle (i.e., asymptotic angle of hyperbolas) by using the distance Δz [shown in Fig. 2(a)] to determine an average distance (i.e., $\Delta z/2$) between the innermost hyperbolas and $z = 0$. Plotting $\Delta z/2$ versus ρ and using the relation $\tan\theta_c = d\rho/d(\Delta z/2)$ then gave θ_c. Figure 3 shows $\sin\theta_c$ plotted versus frequency[9]; this functional dependence constitutes the first experimental demonstration of $\omega < \omega_{ci}$ resonance cone behavior.

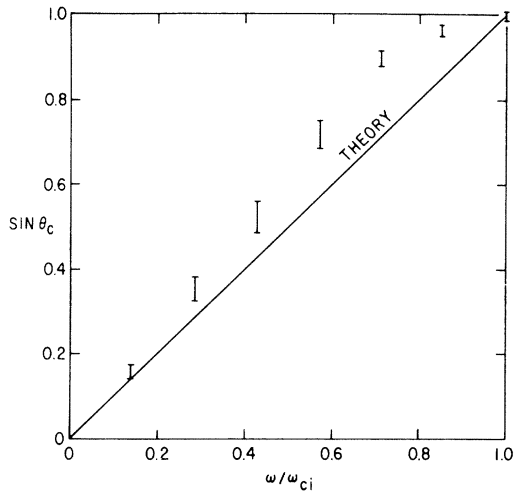

FIG. 3. $\sin\theta_c$ versus ω/ω_{ci} obtained by varying ω.

Finally, to confirm the dependence of the field geometry on ω_{ci}^{-1}, interferometer measurements were made for the same ω as Fig. 2(a) but with a different ω_{ci}. These measurements, an example of which is shown in Fig. 4, again demonstrate the transition from hyperbolic surfaces when $\omega/\omega_{ci} < 1$ to elliptic surfaces when $\omega/\omega_{ci} > 1$.

To summarize, for $\omega < \omega_{ci}$ the surfaces of constant phase are hyperbolic; when ω increases, the asymptotic (i.e., cone) angle $\theta_c \simeq \sin^{-1}(\omega/\omega_{ci})$ of the hyperbolas [cf. Fig. 1(a)] increases until at $\omega = \omega_{ci}$, $\theta_c = \pi/2$. Also, when $\omega < \omega_{ci}$ so that $\theta_c < \pi/2$, there exists an evanescent region for angles $\theta > \theta_c$. For $\theta = 0$ the wave phase corresponds to the low-frequency ion acoustic mode. For ω

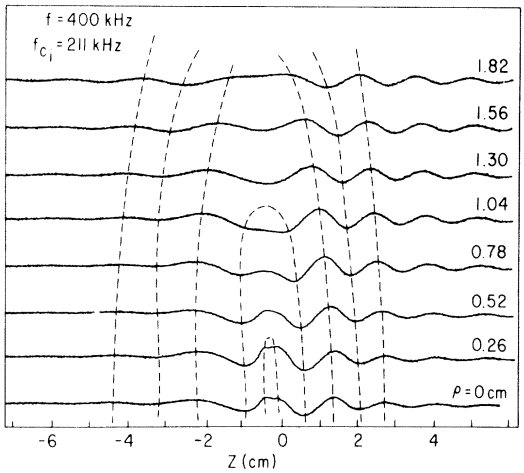

FIG. 4. Same as Fig. 2(a) except that ω_{ci} is changed to give $\omega/\omega_{ci} = 1.90$. Constant-phase surfaces are now ellipses. $B = 555$ G.

$> \omega_{ci}$ the surfaces of constant phase become ellipsoids with major axis aligned perpendicular to $\vec{B}$, as shown in Fig. 1(b). For $\omega > \omega_{ci}$ and $\theta = \pi/2$ the phase given in Eq. (6) corresponds to electrostatic ion cyclotron waves. For $\omega \gg \omega_{ci}$ the surfaces of constant phase become spheres corresponding to isotropic ion acoustic waves, $\omega = kc_s$. Experimental measurements provide strong confirmation for this picture.

The author acknowledges a useful discussion with M. Ono and also thanks J. Johnson and J. Taylor for their technical assistance.

*Work supported by U. S. Energy Research and Development Administration Contract No. E(11-1)-3073.

[1]H. H. Kuehl, Phys. Fluids 17, 1636 (1974).

[2]K. H. Burrell, Phys. Fluids 18, 897 (1975).

[3]T. Ohnuma *et al.*, Phys. Rev. Lett. 30, 535 (1973).

[4]A. Hirose *et al.*, Phys. Fluids 13, 2039 (1970).

[5]R. K. Fisher and R. W. Gould, Phys. Fluids 14, 857 (1971).

[6]K. N. Stepanov, Zh. Eksp. Teor. Fiz. 35, 1155 (1958) [Sov. Phys. JETP 35, 808 (1959)].

[7]A. Erdelyi, W. Magnus, F. Oberhettinger, and F. Tricomi, in *Tables of Integral Transforms*, edited by A. Erdelyi; (McGraw-Hill, New York, 1954), Vol. II, p. 35, Eqs. (20) and (23), and p. 39, Eq. (45), and p. 40, Eq. (48).

[8]P. Bellan and M. Porkolab, Phys. Fluids 19, 995 (1976).

[9]A simultaneous work [T. Ohnuma *et al.*, Phys. Rev. Lett. 37, 206 (1976)] claims that (1) θ_c saturates at $< 90°$ when $\omega \to \omega_{ci}$, and (2) an involved group-velocity angle ($v_{g\perp}/v_{g\parallel}$) dependence on T_i/T_e explains this. The following should be pointed out: (a) Despite similar parameters, no such saturation was observed here, cf. Fig. 3. (b) Ohnuma *et al.*, by probing only downstream of their transmitter (cf. their Figs. 1 and 2), overlooked plasma drift effects. This may explain their observed $< 90°$ saturation, since downstream a drift cause an *apparent* θ_c reduction and $< 90°$ saturation [cf. $z < 0$ of Figs. 2(a) and 2(b) here]. (c) Finite T_i/T_e makes $v_{g\perp}/v_{g\parallel}$ k dependent; thus the one-one correspondence of $v_{g\perp}/v_{g\parallel}$ to θ_c (for which k is undefined) ceases. Although unstated, Ohnuma *et al.*, must have chosen a k for the curves for finite T_i/T_e in their Fig. 3.

Interpretation of Precursors of Internal Disruptions

André Rogister and Günter Hasselberg

Institut für Plasmaphysik der Kernforschungsanlage Jülich GmbH, Association EURATOM-Kernforschungsanlage 5170 Jülich, Federal Republic of Germany

(Received 28 June 1976)

A collisional instability driven by electron temperature gradients is described which appears to explain the major characteristics of the precursors of the internal disruptions. The threshold is reached when a certain parameter $|\mu| > \sqrt{3}$. For the ST and TFR tokamaks, we estimate $1 \lesssim |\mu| \lesssim 5$ at the radius where $q = 1$. For $|\mu| = 3$, the theoretical growth rate $\gamma_{th} \sim (2-3) \times 10^3$ sec^{-1} compares well with the experimental value $\gamma_{exp} \sim 3 \times 10^3$ sec^{-1}. The predicted shape of the wave profile is also in qualitative agreement with experiment.

One of the remarkable features of tokamak discharges is the occurrence of internal plasma disruptions[1-3] which are accompanied by $m = n = 1$ "precursors." Existing theories have attempted to explain the precursors by internal kinks[4] and tearing modes.[5] It appears, however, that the problem is not completely resolved as yet.

The most usual interpretation seems to be that the precursors trigger the internal disruptions, the main observable characteristic of which is a flattening of the temperature profile. This leads us to believe that the precursor should be a temperature-gradient-driven instability since quasilinear theory, usually, predicts self-healing of the plasma. Internal kinks and "standard" tearing modes are not, according to this reasoning, proper candidates to explain the precursors. It is worth noting in this connection that the growth rates predicted in Ref. 4 disagree by almost an order of magnitude with the observations of Ref. 1, while Hazeltine, Dobrott, and Wang[5] come to the conclusion that, among different tearinglike instabilities, a "thermoelectric" mode is the most serious candidate, giving plausible growth rates in particular. Unfortunately effects of finite Larmor radius are completely ignored in this paper, although estimates for present tokamak parameters indicate that the resistive layer is barely 1 ion Larmor radius thick.

We propose here that another instability, specifically a temperature-gradient-driven collisional drift wave (it is noted, however, that trapped-